[Short title + Author Name - P&H title] 17 (2024) 105800

Contents lists available at ScienceDirect

Arabian Journal of Chemistry

journal homepage: www.ksu.edu.sa

Bimetallic PdNi catalyst on cattail Leaves-Derived nanoporous carbon support for synthesis of partially hydrogenated fatty acid methyl ester (H-FAME)

Tripob Longprang [a], Napat Kaewtrakulchai [b], Worapon Kiatkittipong [c], Atthapon Srifa [d], Nuwong Chollacoop [e], Apiluck Eiad-Ua [g,*], Suttichai Assabumrungrat [a,f]

[a] Center of Excellence in Catalysis and Catalytic Reaction Engineering, Department of Chemical Engineering, Faculty of Engineering, Chulalongkorn University, Bangkok, 10330, Thailand
[b] Biomass Conversion and Bioenergy Research Unit, Kasetsart Agricultural and Agro-Industrial Product Improvement Institute, Kasetsart University, Bangkok 10900, Thailand
[c] Department of Chemical Engineering, Faculty of Engineering and Industrial Technology, Silpakorn University, Nakhon Pathom, 73000, Thailand
[d] Department of Chemical Engineering, Faculty of Engineering, Mahidol University, Nakhon Pathom, 73170, Thailand
[e] National Energy Technology Center, Thailand Science Park, Pathumthani, 12120, Thailand
[f] Bio-Circular-Green-economy Technology & Engineering Center, BCGeTEC, Department of Chemical Engineering, Faculty of Engineering, Chulalongkorn University, Bangkok, 10330, Thailand
[g] College of Materials Innovation and Technology, King Mongkut's Institute of Technology Ladkrabang, Ladkrabang, Bangkok, 10520, Thailand

ARTICLE INFO

Keywords:
Cattail leaves
Mesoporous carbon
Chemical activation
Hydrothermal carbonization
Partial hydrogenation
H-FAME

ABSTRACT

Cattail leaves (CL) have been used as a carbon source to synthesize nanoporous carbon (NPC) support with high surface area (S_{BET} = 2002.12 m^2g^{-1}) via hydrothermal carbonization and potassium hydroxide (KOH) activation. The studied catalysts, including monometallic Pd/NPC and Ni/NPC, and bimetallic PdNi/NPC, were synthesized and characterized by using several techniques (e.g., scanning electron microscopy, transmission electron microscopy, nitrogen sorption, Fourier transform infrared spectroscopy, thermogravimetric analysis, and X-ray diffraction). Their catalytic activity toward partial hydrogenation of palm biodiesel to H-FAME was tested, and the liquid product composition, cloud point, and oxidation stability were determined. The studied catalysts have a high porosity with the S_{BET} of approximately 2037.34–2187.96 m^2g^{-1} led to excellent metal dispersion. Although Ni did not show high catalytic activity compared to Pd, Ni incorporated with Pd as PdNi/NPC catalyst significantly increased the *cis*-C18:1 selectivity and prevented the catalytic deactivation during the partial hydrogenation. The oxidation stability of palm biodiesel feedstock was increased from 13.69 to 17.12 h while the cloud points adversely increased by only 3 degrees from 12 to 15 °C (still lower than 16 °C of the Thai industrial recommendation) with bimetallic PdNi/NPC catalyst. The main benefit of bimetallic PdNi/NPC over monometallic Pd/NPC and Ni/NPC is shown through not only higher C18:2 conversion but also much higher *cis*-to-trans ratio of C18:1 resulting in higher oxidation stability with acceptable compromise on the cloud point increasing. Consequently, the produced palm H-FAME can be used at a high blend ratio.

1. Introduction

Despite being one of the most unsustainable sources, petroleum is widely used as a feedstock for the production of various fuels such as gasoline, liquid petroleum gas, jet fuel, heavy fuel oil, kerosene, and especially diesel (Nelson, 2018). Nowadays, industries and agriculture, including transportation section, are growing extensively, so the desire for power sources for engines and machinery has sharply increased (Knothe, 2010; Murugesan et al., 2009). Due to concern about depleting global fossil fuels, the role of renewable energy has recently increased. Biodiesel is one of the most promising and simple renewable sources to replace diesel due to its comparable calorific value to diesel fuel, better engine lubrication, and low environmental impact (Huang et al., 2012; Knothe, 2010; Murugesan et al., 2009). Conventionally, biodiesel is

* Corresponding author.
E-mail address: apiluck.ei@kmitl.ac.th (A. Eiad-Ua).

https://doi.org/10.1016/j.arabjc.2024.105800
Received 18 December 2023; Accepted 15 April 2024
Available online 16 April 2024

produced via transesterification and esterification by reacting triglyceride and fatty acid molecules with alcohol. However, biodiesel synthesized from transesterification faces challenges in terms of oxidation stability and cold flow properties compared to diesel (Nabi et al., 2006; Vedaraman et al., 2011). To solve this problem, a small proportion of biodiesel is added to diesel (e.g., 10 percent (B10) and 20 percent (B20)) to adjust the fuel properties of biodiesel-blended diesel within acceptable standards (Turrio-Baldassarri et al., 2004). To increase blending ratio, partial hydrogenation plays a vital role in improving biodiesel's fuel properties.

Partial hydrogenation is a standard method to directly improve biodiesel oxidation stability without significantly jeopardizing cold flow property by adding hydrogen atoms to the double bonds of C18:2 and C18:3 polyunsaturated FAME structure to maximize the monounsaturated FAME (C18:1) in hydrogenated biodiesel (H-FAME). H-FAME biodiesel can be used as a standalone or mixed with diesel (Adu-Mensah et al., 2019). In this reaction, heterogeneous catalysts are preferred due to their potentially low cost and reduction of water required for catalyst separation and cleaning, resulting in an effective decrease of catalyst treatment system costs compared to homogeneous catalysts (Boreskov, 2003; Satterfield, 1991).

Noble transition metals such as palladium (Pd) and platinum (Pt) are commercially used as the active phases of catalysts in partial hydrogenation of FAMEs due to their high catalytic activity at low temperatures and pressures (Numwong et al., 2013; Stathis et al., 2017). In addition, palladium has good selectivity in cis–trans isomerization to promote isomerization of the C18:1 structure, increasing biodiesel's cold flow properties due to its crystallization point (Quaranta & Cornacchia, 2020). Although palladium (Pd) and platinum (Pt) have good catalytic activity, industrial production would prefer to reduce the amount of noble metal catalysts due to their high cost (Tang et al., 2022; Zhu et al., 2018). To solve this problem, transition nanometal catalysts such as nickel (Ni), copper (Cu), cobalt (Co), sodium (Na), magnesium (Mg), calcium (Ca), barium (Ba), and iron (Fe) (Alshater et al., 2023; Aly & Fathalla, 2020; Hosny et al., 2024) have been considered instead due to their lower costs compared to commercial metal catalysts (Pd and Pt) and some additional properties such as sulfur tolerance (Numwong et al., 2013; Thunyaratchatanon et al., 2018). Although the cost of transition nanometal catalysts is lower than palladium and platinum, it provides much lower catalytic activity (Abdalla et al., 2021; Aly & Elembaby, 2020). Furthermore, adding some noble metals remains a common practice for increasing activity instead of standalone non-noble metal catalysts. In the past few years, bimetallic forms, such as Pd/Pt (Na Rungsi et al., 2021), Pd/Ni (Fiore et al., 2022; Trisunaryanti et al., 2022), CoMo (Putri Afifa Nur Oktadina, 2023), and Rh/Mo (Huang et al., 2020) have been researched and developed because researchers need to use the synergistic effect of bimetallic forms to enhance catalyst properties such as catalyst lifetime, sulfur resistance and dispersion of active metals, which altogether improve catalyst stability and prevent catalyst deactivation (Sinfelt, 1985; Toshima & Yonezawa, 1998). Therefore, the deactivation of catalysts in the production process is a major concern in the industry, which could affect operating costs by shutting down production systems to regenerate the deactivated catalyst into fresh catalysts. Catalyst deactivation is caused by several factors, such as operating conditions that directly affect the catalyst, deterioration of some components, and contaminated elements (sulfur content) in raw materials (Edvardsson et al., 2001; Piccolo & Kibis, 2015). Catalyst support also plays an important role in catalyst efficiency. The commercial supports used in industrials are, for example, silica, zeolite, alumina, and carbon materials, which exhibited low support to metal interaction that affects the dispersion of active phases onto the support surface. Silica and alumina supports are synthesized from inorganic substrates through several complex methods, which often need to be more environmentally friendly due to chemical waste from the synthesis process (Adu-Mensah et al., 2019). For Instance, Pd/C has been effectively used as a catalyst for the partial hydrogenation of tobacco seed oil-derived biodiesel (Eugenio Quaranta, 2022) and for upgrading fish oil derived biodiesel (Studentschnig et al., 2015).

Regarding nanoporous carbon, the process of producing nanoporous carbon usually consists of two steps: char production from raw material and char activation for pore growth (Jadsadajerm et al., 2024; Kaewtrakulchai et al., 2023). Physical and chemical activations are the two categories into which the activation process is divided (Kaewtrakulchai et al., 2024; Panomsuwan et al., 2022). A physical activating agent environment, such as steam and carbon dioxide, is fed into the process during physical activation, typically carried out at temperatures above 800 °C. This simultaneously catalyzes the partial gasification of a char precursor, which has demonstrated that physical activation has some benefits, including simple operation and little secondary waste production. This process should be highlighted, nonetheless, that the final product frequently has a high ratio of microporous structure and a modest surface area less than 1000 m^2/g (Chanpee et al., 2022). Chemical activation usually involves two different steps. The first stage involves impregnating a carbonaceous material with a chemical compound, such as phosphoric acid (H_3PO_4), zinc chloride ($ZnCl_3$), sodium hydroxide (NaOH), or potassium hydroxide (KOH). The generated sample was then carbonized at a moderate temperature range of 500 to 800 °C (Kaewtrakulchai et al., 2022a). Nanoporous carbon has demonstrated significant benefits in adsorption and separation. Recent studies have shown that nanoporous carbon can be used in various energy applications, including as biocatalysts and catalyst support materials and in energy storage devices (Siddiqui et al., 2021; Tran et al., 2020; Vignesh et al., 2021; Wang et al., 2018). However, the use of nanoporous carbon as a support for metal catalysts in catalysis routes enhances the generation of biofuels and biochemicals due to its advantageous pore structure, numerous surface-active sites, and expansive surface area (Roy et al., 2022). Porous carbons are optimal and effective substrates for hydrotreating catalysts. Their exceptional pore properties enabled the efficient dispersion of the nanometal catalyst (Khalit et al., 2020; Kaewtrakulchai et al., 2020).

Therefore, this study aimed to synthesize nanoporous carbon support (NPC) from cattail leaves with high specific surface area and explore the NPC as a catalyst support applied for the partial hydrogenation of palm oil biodiesel. Herein, the NPC synthesized from the conventional method exhibited a very high surface area and pore volume compared to commercial support. The second purpose of this research is to synthesize the bimetallic PdNi supported on nanoporous carbon support derived from cattail leaves as raw material, followed by identifying optimal conditions in partial hydrogenation of palm biodiesel to H-FAME via such catalysts.

2. Materials and methods

2.1. Materials

Cattail leaves (CL) were collected from waterlogged areas in King Mongkut's Institute of Technology Ladkrabang (KMITL) in Thailand. Potassium hydroxide (KOH) anhydrous pellets (Sigma-Aldrich, USA) were used as an activating agent. Palm biodiesel (B100), a biodiesel feedstock for partial hydrogenation, was obtained from Patum Vegetable Oil Company Limited (Pathum Thani, Thailand).

2.2. Preparation of cattail Leaves-Derived nanoporous carbon

CL was a carbon source to prepare nanoporous carbon (NPC). CL was dried at 110 °C before being cut and meshed into powder. The CL powder was sieved to achieve a particle size of 2 μm. To produce hydrochar (HC), 30 g of CL was mixed with 60 ml of DI water and then packed into the autoclave to hydrothermal at 200 °C for 12 h. After the hydrothermal reaction, the autoclave was quickly cooled to room temperature to stop the reaction immediately. Hydrochar (HC) was dried at 90 °C for 12 h to ensure that the water was eliminated. Chemical

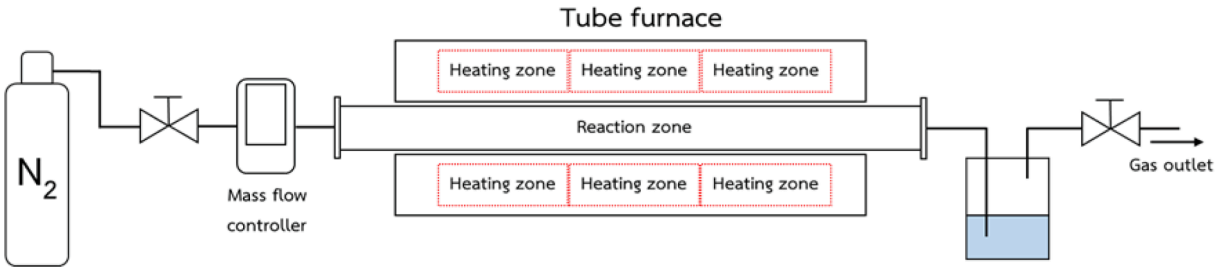

Fig. 1. Schematic diagram of a horizontal tube furnace for chemical activation of cattail leaves for production of nanoporous carbon.

activation was used to promote the porosity of nanoporous carbon following our previous study (Kaewtrakulchai et al., 2022a). HC of 10 g was stirred in 4 M KOH solution at 80 °C for 2 h. The mixture of HC was filtrated using a Buchner funnel with the vacuum pump and then dried to evaporate water in the solution. After that, the dried HC was placed in a horizontal tube furnace for carbonization at 900 °C for 2 h with 100 ml/min of nitrogen flow rate and a heating rate of 10 °C/min using the horizontal tube furnace, as seen in the schematic diagram in Fig. 1. Finally, nanoporous carbon (NPC) was washed with 0.5 M of HCL and distilled water until achieving a pH of 7, followed by drying at 110 °C for 24 h for further characterization and application as a catalyst supporter.

2.3. Preparation of PdNi/NPC catalyst

Nanoporous carbon was used as a support material for catalysts. Tetraamminepalladium (II) chloride monohydrate [$Pd(NH_3)4{\cdot}Cl_2{\cdot}H_{20}$] and Nickel (II) nitrate hexahydrate [$Ni(NO_3)_2{\cdot}6H_2O$] (98 % purity) were used as metal precursors. Catalysts were synthesized by wet impregnation technique (Douvartzides et al., 2019). Monometallic catalysts (Pd/NPC and Ni/NPC) were prepared by using 1 wt% for Pd and 5 wt% for Ni catalyst due to its lower catalytic activity. Bimetallic catalyst (PdNi/NPC) was prepared by using mixture of Pd and Ni at 1 % and 5 % of metal catalysts, respectively. Metal precursor solutions were mixed with 10 g of nanoporous carbon at temperature of 60 °C and dried by using a rotary evaporator with vacuum atmosphere until completely evaporated. After that, the catalysts were calcined at 500 °C for 3 h under nitrogen atmosphere at a heating rate of 10 °C/min. The metal oxide species was obtained from the calcination process. Before catalyst characterization and reaction testing, the prepared metal oxide catalysts were reduced at the temperature of 500 °C for 6 h under H_2 flow of 100 mL/min to transform the metal oxide into metallic catalyst form (Kaewtrakulchai et al., 2022b).

2.4. Characterization

2.4.1. Characterization of nanoporous carbon

As described above, nanoporous carbon from cattail leaves synthesized through hydrothermal carbonization (HTC) was used as a catalyst support. The characteristics of NPC have been investigated by proximate and ultimate analysis, Fourier transform infrared spectroscopy (FTIR), Thermogravimetric analysis (TGA), Scanning electron microscope (SEM), and Nitrogen sorption technique. The specifications of the characterization techniques are explained as follows.

Fourier transforms infrared (FTIR) spectroscope was used to investigate the surface functional group to specify the organic and inorganic molecules by the vibration of bonds while adsorbing wavelength in the infrared range. Surface functional groups were analyzed by PerkinElmer UATR Two using ATR transmission mode. The samples were packed and pressed onto ATR crystal material. IR scan was used in a range of 400 to 4,000 cm^{-1} with 8 cycles of scan rate.

Netzsh TG 209 F3 Tarsus used thermogravimetric analysis (TGA) to analyze the thermal stability and decomposition of sample compositions. The samples were scanned at a temperature range of 26–900 °C and a heating rate of 10 °C/min under a nitrogen atmosphere. The proximate analysis result, including moisture, volatile matter, fixed carbon, and ash was calculated by TG profile. The ultimate analysis (C, H, N percentages) was determined by a LECO Truspec CHN628 analyzer. The O percentage was directly calculated by subtraction of other compositions from 100%.

A scanning electron microscope (SEM; Zeiss MA10) was used to analyze the catalyst morphology and obtained support. The samples were attached with carbon tape and put onto specimen stubs. Then, samples were coated with gold (Au) by sputtering under a vacuum atmosphere to enhance electrical conductivity on the sample surface. The coated samples were scanned in secondary electron mode and operated at 10 kV. the magnification used at 500x, 1000x to receive high resolution images.

The textural pore properties were determined at −196 °C using N_2 sorption analyzer, the Quantachrome Autosorp iQ-MP-XR. The samples were degassed at 300 °C for 4 h before to sorption analysis. The specific surface area was estimated using the Brunauer-Emmett-Teller (BET) model for relative pressures ranging from 0.1 to 0.99 (Ahmad et al., 2020). The Barrett-Joyner-Halenda (BJH) method was used to compute the total pore volume at saturated pressure. The density functional theory (DFT) model investigated the pore size distribution (Naseem et al., 2023).

2.4.2. Characterization PdNi/NPC catalyst

Different techniques were used to investigate the characteristics of prepared catalysts, such as X-ray diffraction (XRD), Scanning electron microscope (SEM), Energy dispersive spectrometry (EDS), Transmission electron microscope (TEM), N_2 adsorption/desorption, and CO chemisorption. The specifications of characterization techniques are explained below.

X-ray diffraction (XRD) technique was used to investigate crystallinity, identify crystal structure and crystallite size, and confirm the metal formed on the surface of prepared catalysts. X-ray diffractograms were obtained using the Rigagu Smartlab X-ray diffractometer with Guidance software. The x-ray source is Cu-Kα radiation (λ = 1.5418 A°) with an accelerating voltage of 40 kV and a current of 40 mA. X-ray sources and detectors scanned from 10 to 90° with theta-2-theta mode in a step of 0.02°/s. The Debye-Scherrer equation can determine the crystallite size of the catalyst.

Energy dispersion spectrometry (EDS) was performed to identify the elemental distribution on the surface and quantitatively analyze the catalyst. The elemental analysis of the catalyst can be determined by X-ray fluorescence analysis. Results were shown in atomic ratio and color mapping.

Metal dispersion on the catalyst was performed using Ohkura Riken R6015-S, expressed as the ratio of the total number of metal atoms on the metal surface. Metal dispersion was calculated by assuming that the atomic ratio of CO to the metal surface is 1:1. The U-quartz tube reactor contained 0.03 g of quartz wool and 0.1 g of catalyst. The samples were reduced at the same temperature with H_2-TPR at a 25 mL/min flow rate using a heating rate of 10 °C/min for 3 h before cooling down to 25 °C in a nitrogen flow. The CO injected 20 μL until absorption saturation was

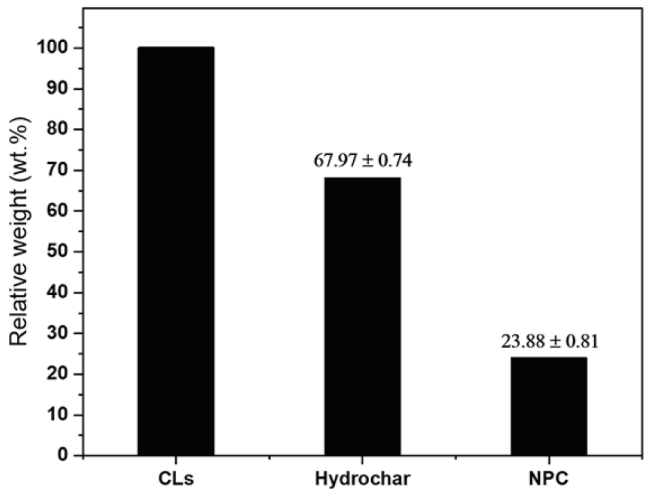

Fig. 2. Yields of CL, CL hydrochar and NPC.

obtained at 30 °C. A thermal conductivity detector (TCD) observed by a mass spectrometer detected the CO output gas. The amount of CO adsorption was calculated by the difference between the CO amount detected at the outlet and the amount of CO injected at the inlet. The cubic particle model was used to calculate the catalyst particle size and metal distribution on the catalyst.

Transmission electron microscopy (TEM) analysis was used to identify the internal morphology and loaded metal catalyst particles on catalyst support. JEOL TEM-2100Plus obtained TEM micrographs with an accelerating voltage of 200 kV. The sample was sonicated to be suspended in ethanol and then dropped onto carbon-coated copper grids. Image J (National Institutes of Health (NIH), Bethesda, MD, USA) software analyzed the distribution of metal particle sizes.

2.5. Partial hydrogenation of palm biodiesel

The catalysts were reduced at 300 °C (Pd) and 400 °C (Ni and PdNi) for 2 h. Partial hydrogenation of biodiesel was conducted in a 300 ml batch-type reactor. First, 200 ml of biodiesel produced from palm oil feedstock and 1.75 g of catalyst were added to the autoclave. The reactor was subsequently flushed with nitrogen to remove air in the reactor. The samples were collected every 30 min for a total reaction time of 4 h for the analysis of product distribution and partial hydrogenation performance (Eugenio Quaranta, 2022; Studentschnig et al., 2015).

2.6. Analysis of palm H-FAME

The compositions of biodiesel feedstock and liquid product after hydrogenation were analyzed using gas chromatography with a flame ionization detector (GC-FID, GC-2010) equipped with a capillary column (HP-88, 100 m x 0.25 mm x 0.2 μm). Helium was a carrier gas with a flow rate of 53.8 mL/min. A sample of 1 μL was injected into an oven at 170 °C after 40 min. The temperature was increased to 230 °C with a heating rate of 4 °C/min. The detector temperature was fixed at 250 °C with a 50:1 split ratio. The FAME compositions were identified by comparison with standards. The ratio of the area under the peak was used to calculate the FAME compositions.

The oxidation stability of the biodiesel before and after partial hydrogenation was analyzed by Rancimat 743. The flask containing a 7.5 g sample was heated to 110 °C with 10 L/h of air. The air was passed through the sample and then fed into a collection vessel containing a 60 mL DI and conductivity probe. The oxidation stability of sample was presented in terms of induction period (IP). The IP explained the difference in time between the start of the test and conductivity, which increases immediately in the collective flask. Typically, the IP value is expressed for time and long IP times of biodiesel fuel, indicating high stability against oxidation.

The cold flow properties of the biodiesel before and after partial hydrogenation were expressed in terms of cloud point and pour point, which were examined using the Tanaka MPC-102 Tech pour/cloud tester developed by ASTM D6749. 70 mL of biodiesel was added to the tester glass flask. The biodiesel sample was cooled to less than 0 °C and then heated until it reached 45 °C. After the experiment, the sample was cooled to room temperature before the sample was collected.

3. Results and discussion

3.1. Characteristics of the cattail leaves derived NPC materials and PdNi/NPC catalyst

The yields of cattail leaves (CL), CL hydrochar, and CL-derived NPC are shown in Fig. 2. CL hydrochar was produced from a hydrothermal process operated at 200 °C for 24 h. The heat and pressure in the autoclave allow the water molecule to diffuse and decompose the organic compound (cellulose, hemicellulose, and lignin) in CL structures, which causes the long-chain polymer to break into a short-chain polymer and then decompose into gases such as hydrogen (H_2), carbon monoxide (CO) and carbon dioxide (CO_2), forming the carbon atom. The yield of CL hydrochar was approximately 67.97 wt%. After the activation process, 23.88 wt% of NPC yield could be achieved because of the concentration of the activating agent, leading to an increase in activation degree (Li et al., 2017). Furthermore, the existing KOH activating agent at high activation temperature directly caused the oxidation of the hydrochar precursor. This activation reaction transformed carbon atoms into tar and other pyrolytic gases, such as hydrogen (H_2), oxygen (O_2), nitrogen (N_2), and methane (CH_4) released from the carbon matrix, causing pore cavities, thus increasing a high surface area.

The proximate and ultimate analysis of CL, CL hydrochar, and CL-derived NPC is shown in Table 1. It can be separated into moisture, volatile matter, fixed carbon, and ash. The fixed carbon and ash content is the main component in CL because the carbon atom is the main component of organic substances, and ash plays a significant role in various utilization (Tseng et al., 2008). Hydrochar was produced from the cattail leaves through hydrothermal processes, where the volatile matter in the CL structure (cellulose, hemicellulose, and lignin) decreased with increasing fixed carbon content. After activation and carbonization, NPC was produced, and upon complete carbonization, fixed carbon, and ash content also increased from the evaporation of

Table 1
Proximate and ultimate analysis of cattail leaves (CL).

Properties	Proximate analysis (wt.%) [a]				Ultimate analysis (wt.%) [b]			
	M	VM	FC*	A	C	H	N	O*
Raw CL	1.58	75.90	20.31	2.21	39.95	4.46	1.74	53.85
Hydrochar	1.63	62.31	33.28	2.78	45.45	45.45	45.45	45.45
NPC	1.59	10.41	81.18	6.82	86.35	4.67	1.64	7.34

* Calculated by difference, M: moisture, VM: volatile matter, FC: fixed carbon, A: ash.
[a] As-received basis,
[b] Dry-Ash-Free basis.

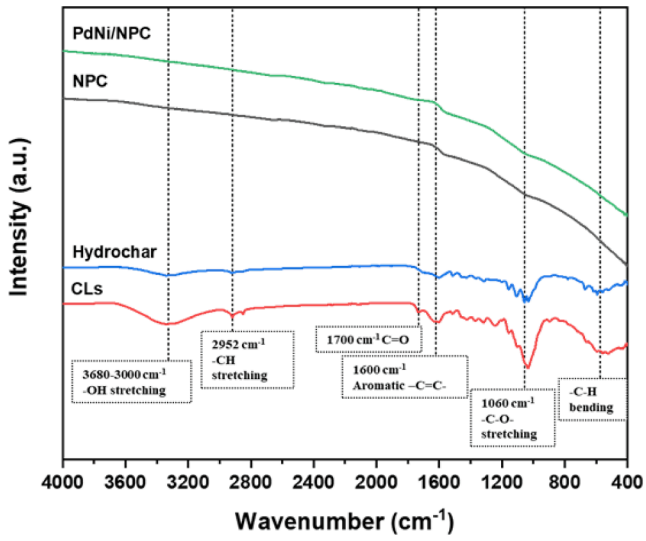

Fig. 3. Fourier transform infrared spectroscopy (FTIR) spectra of CL-derived NPC and post-loaded catalyst.

Table 2
Functional groups of the CL, CL hydrochar, CL-derived NPC and PdNi/NPC.

Wavenumber (cm^{-1})	Functional group	Description
3680—3000	O–H stretching	Hydroxyl or carboxyl groups, alcohols from cellulose or phenols from lignin
3000—2800	C–H stretching	Aliphatic
1700	C = O stretching	Carbonyl, ester or carboxyl from cellulose and lignin
1600 and 1512	C = C stretching	Aromatic skeletal present in lignin
1380—1240	C-O stretching	Vibration in lignin
1290—950	C-O stretching	Hemicellulose esters
1420	C–H bending	C–H deformation in lignin and carbohydrates
1060	C-O stretching	Vibrations in cellulose and hemicellulose
860—724	C–H bending	Aromatic

volatile matter. Fixed carbon observed in the proximate analysis was gradually increased from 33.28 to 81.18, yielding activated carbons with fixed carbon content over 70 % and 2–10 % for ash content. Increasing ash represented the decrease of porosity, leading to decreased specific surface area from the carbon matrix (Dizbay-Onat et al., 2017; Manoj & Kunjomana, 2012).

Fig. 3 exhibits the functional groups on the surface of the CL raw material, CL hydrochar, CL-derived NPC, and PdNi/NPC catalysts, while Table 2 provides FTIR band assignments of these materials. It was indicated that after undergoing the hydrothermal treatment process at 200 °C for 12 h, the OH-stretching (3680–3000 cm^{-1}) peak was reduced, which is a slight hydroxyl group of lignin due to the high thermal stability of its structure. The reduction of the peak CH-stretching (2925 and 2850 cm^{-1}) from aliphatic degradation and a significant decrease of CO stretching from the ether group of cellulose and hemicellulose (Jaruwat et al., 2018) showed low thermal stability. The decomposition of cellulose and hemicellulose during the hydrothermal process caused an aromatic group structure from aromatization, shown at 1600, 1512, 1460, and 790 cm^{-1} peaks. Additionally, a C = O vibration approximately at 1700 cm^{-1} was formed during the hydrothermal process, which was a component of the carboxylic, ketone, and aldehyde group formed by dehydration of the hydroxyl groups from the decomposition of cellulose and hemicellulose (Yao et al., 2017). After undergoing pore activation and carbonization at 900 °C for 2 h, the structure of cellulose, hemicellulose, and lignin was wholly decomposed. Compared to the pre-

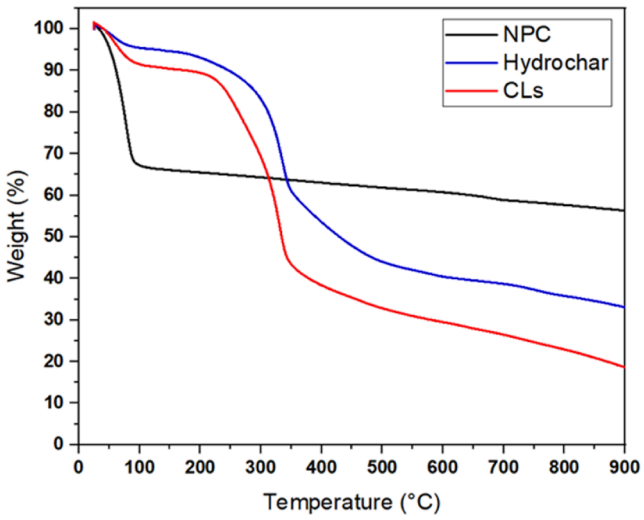

Fig. 4. Thermogravimetric analysis (TGA) of CL, CL hydrochar and NPC.

carbonization period, aromatization directly occurred on the surface due to the decomposition of tar and volatile substances such as hydrogen, oxygen, nitrogen, and water evaporation from the structure within the substance to become porous (Arana et al., 2003; Shin et al., 1997). This phenomenon resulted in the smooth FTIR spectra obtained for NPC and NPC-supported catalysts. However, functional groups of the metal catalyst cannot be observed from the FTIR analyses due to the low resolution of chemical bonding between metal particles and NPC since the metal phase is located on the NPC matrix by the physical formation from the catalyst synthesis (González-Castaño et al., 2021; Kaewtrakulchai et al., 2022a).

The TGA profiles of CL, CL hydrochar, and NPC are shown in Fig. 4. CL and hydrochar curves showed three main stages indicating the pyrolysis process of biomass. The first stage was founded at a low-temperature range (<110 °C), corresponding to the evaporation of moisture content. The second stage (160–400 °C) exhibited the gradual decrease of CL and hydrochar mass caused by the decomposition of cellulose and hemicellulose corresponding to the active pyrolysis. Lignin decomposition occurred at both the second and third stages due to its high thermal stability. The last stage (>400 °C) exhibited a slight decrease in weight loss while temperature increased, which was attributed to the passive pyrolysis process (Manić et al., 2019).

The surface morphology of CL and NPC were examined using the scanning electron microscopy (SEM) technique at magnification of 500x and 2000x, as shown in Fig. 5. CL had no porous structure, and a dense and smooth surface was exhibited on the external surface. After the hydrothermal carbonization (HTC) process, it was indicated that various pores and cavities were dispersed on the surface of the nanoporous carbon support, which was caused by KOH activation (Xiang et al., 2011) due to the high amount of potassium ions, pore expansion, and channeling. The pore size was in the nanopore range, primarily found in mesopores and some micropores at the surface of NPC. The fractured structure occurred due to the high temperature of carbonization and KOH-activated conditions, showing physical fracture from external impact during the process.

The dispersion of the bimetallic PdNi catalyst on the carbon support was 6 wt% at a Pd:Ni ratio of 1:5, as shown in Fig. 6. It was indicated that metallic particles were well dispersed on the surface of the nanoporous carbon support. For qualitative and quantitative analyses, EDX (Energy Dispersive X-ray) demonstrated the pattern and dispersibility of monometallic metals on the surface in the form of colored dots confirming metal catalyst impregnation onto the support surface. The wet impregnation method generated a dispersion pattern of metallic catalyst particles on the surface of NPC. A rotary evaporator has been used to dry

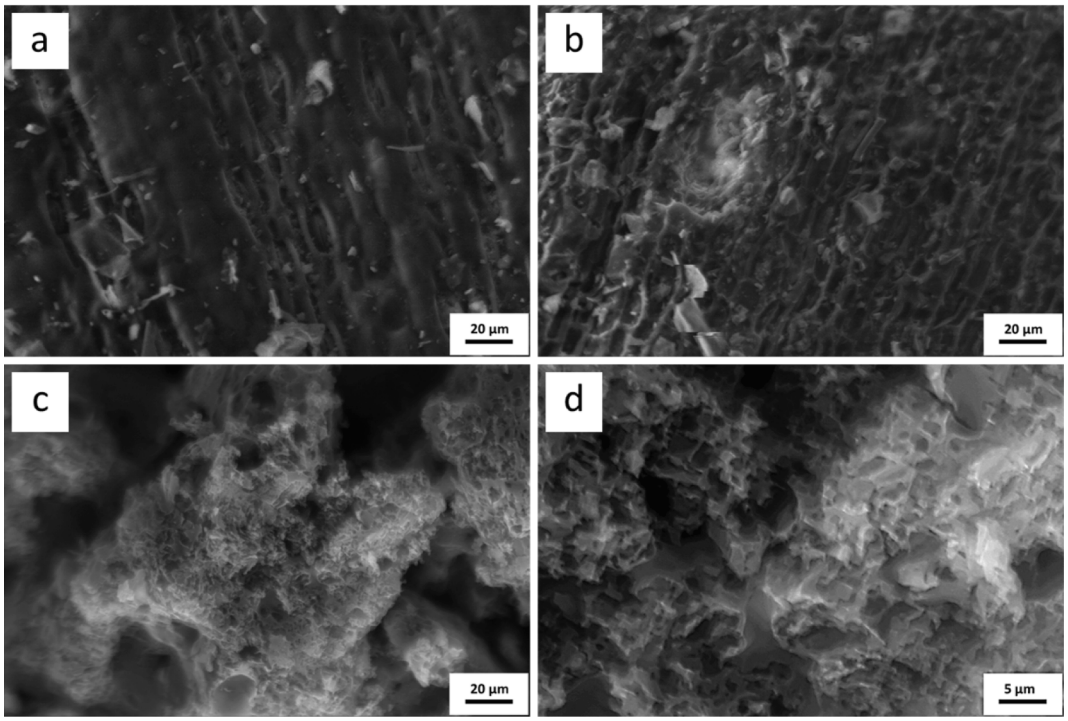

Fig. 5. Scanning electron microscope (SEM) micrographs of (a) CL, (b) CL hydrochar, (c) CL-derived NPC at 500x and (d) 2000x magnification.

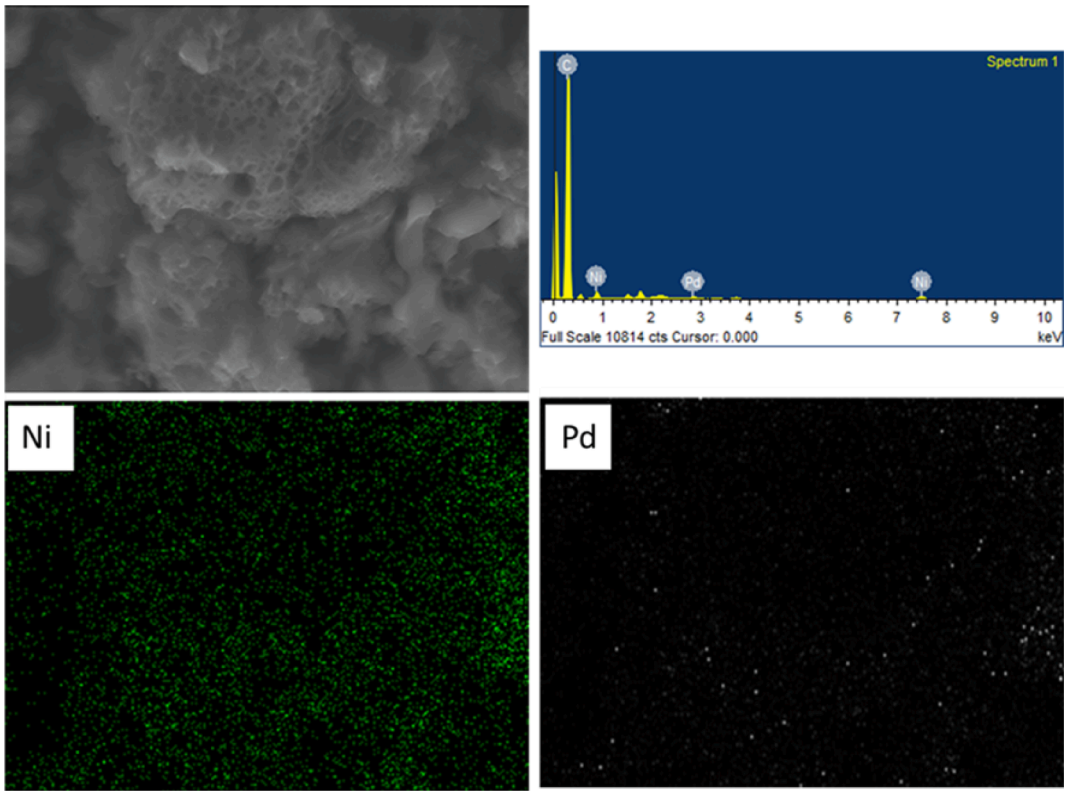

Fig. 6. Energy dispersed X-ray (EDX) spectra of PdNi/NPC.

catalysts, where pressure reduction was applied to allow air to be sucked out of the porous area on the support surface. This finding allowed the solution-type metal particles to flow within the porous area formed on the support surface (Puna et al., 2010).

TEM observed detailed internal morphologies of CL-derived NPC, monometallic catalysts (Pd/NPC and Ni/NPC), and bimetallic catalysts (PdNi/NPC). Moreover, Fig. 7 shows the TEM micrograph indicating a disordered hierarchical porous structure containing innumerable pores (Udomsap et al., 2021). The gaps between disordered carbon layers suggested the existence of mesopores and micropores in NPC. In

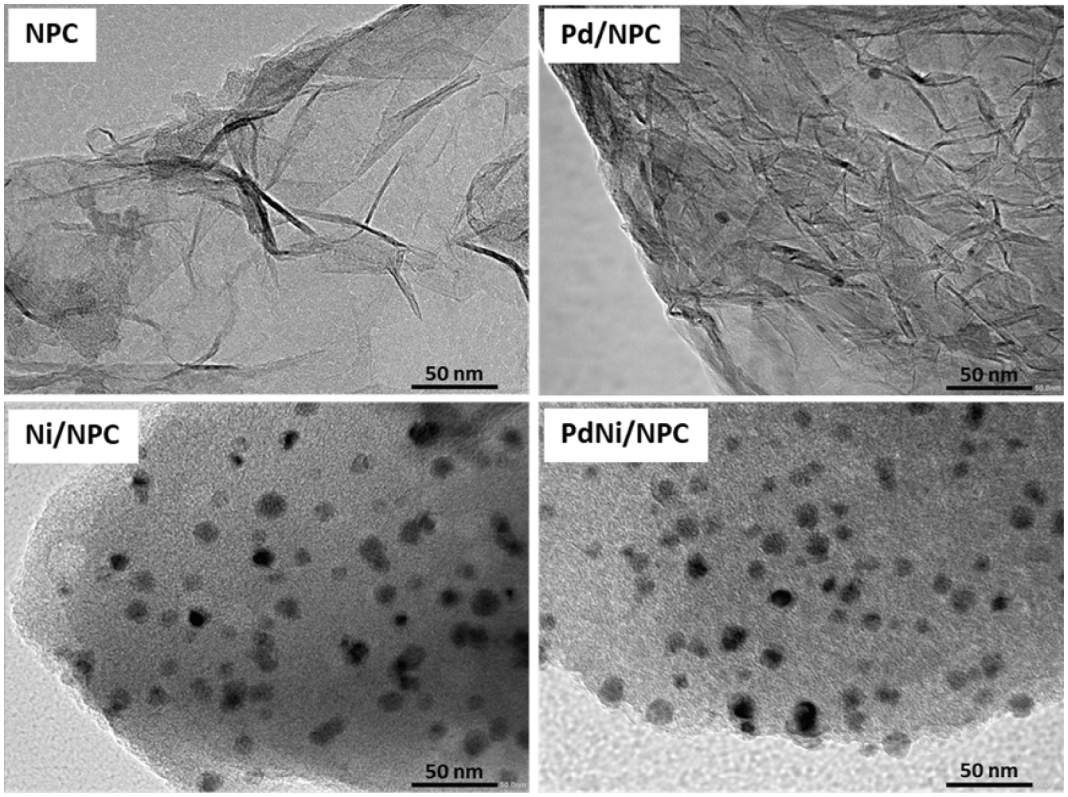

Fig. 7. TEM micrograph of the NPC, Pd/NPC, Ni/NPC and PdNi/NPC catalysts.

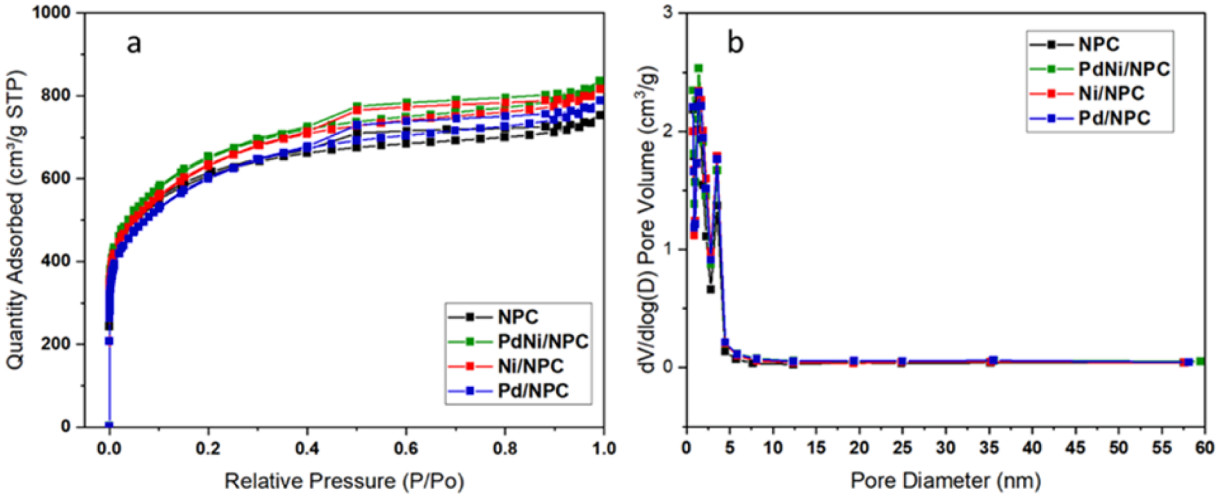

Fig. 8. (a) N2 adsorption and desorption isotherms and (b) pore size distribution of NPC, Pd/NPC, Ni/NPC and PdNi/NPC.

addition, the particle size of metallic Pd, Ni and PdNi on NPC from TEM images were observed at 6.5 ± 1.6 nm, 11.3 ± 1.9 nm and 13.6 ± 0.7 nm, respectively.

The N_2 adsorption and desorption isotherms of bare NPC and metal-loaded NPC are shown in Fig. 8**(a)**. According to the IUPAC classification (Naderi, 2015), The sorption isotherms of NPC support and NPC-supported catalysts exhibited hysteresis loop type IV, indicating the majority of mesopores (2–50 nm) and some micropores (>2 nm) (Tang et al., 2022). With the hysteresis loop, KOH activating at 900 °C for 2 h generated a pore size that is suitable for substances with high viscosity molecules, such as biodiesel and gas reactants, to react with the active site dispersed on the pore surface (Lee & Wilson, 2015). Fig. 8**(b)** shows the pore size distribution of CL-derived NPC, Pd/NPC, Ni/NPC, and

Table 3
Textural pore structure of CL-derived NPC, Pd/NPC, Ni/NPC and PdNi/NPC.

Sample	S_{BET} (m^2g^{-1})	D_{av} (nm)	V_{total} (cm^3g^{-1})	V_{mic} (cm^3g^{-1})	V_{mes} (cm^3g^{-1})
NPC	2002.12	2.63	1.573	0.280	1.239
Pd/NPC	2037.34	2.71	1.601	0.285	1.261
Ni/NPC	2142.16	2.82	1.667	0.296	1.31
PdNi/NPC	2187.96	2.96	1.730	0.308	1.363

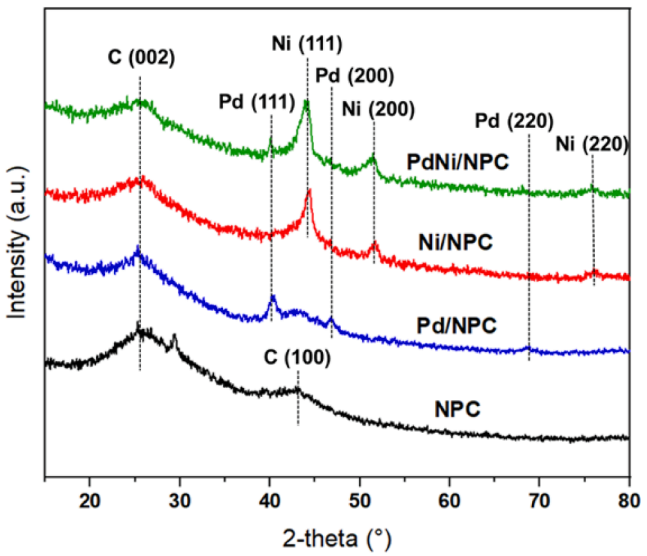

Fig. 9. XRD patterns of the NPC, Pd/NPC, Ni/NPC and PdNi/NPC catalysts.

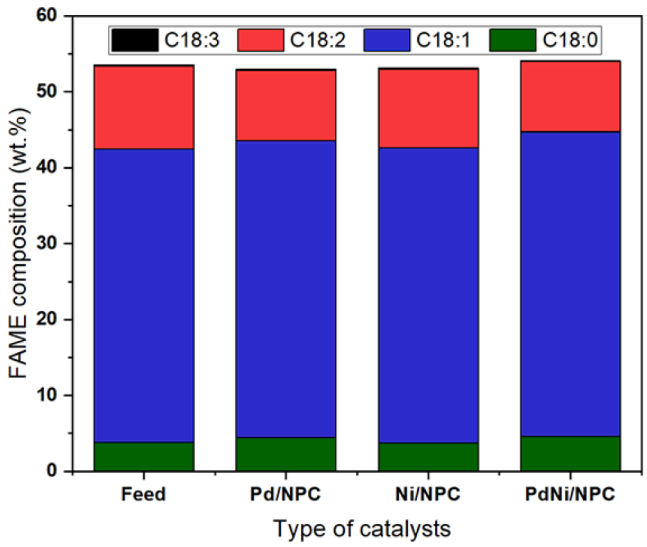

Fig. 10. Effect of monometallic and bimetallic of PdNi on C18 composition (reaction temperature = 100 °C, H_2 pressure = 4 bar and reaction time = 4 h).

Table 4
FAME compositions and biodiesel properties of palm BDF and H-FAME over Pd/NPC, Ni/NPC and PdNi/NPC catalysts (reaction temperature = 100 °C, H_2 pressure = 4 bar and reaction time = 4 h).

FAME composition (wt.%)	Palm BDF	H-FAME		
		Pd/NPC	Ni/NPC	PdNi/NPC
C18:0	3.81	4.42	4.20	4.57
C18:1	38.65	39.16	37.75	40.16
cis-C18:1	38.57	36.61	37.65	39.94
trans-C18:1	0.08	2.76	0.10	0.22
C18:2	10.92	9.29	10.01	9.26
C18:3	0.18	0.14	0.16	0.12
Conversion of C18:2 (%)	–	14.93	5.40	15.20
Biodiesel properties				
Oxidation stability (h.)	13.69	16.33	14.10	17.12
Cloud point (°C)	12	14	14	15

PdNi/NPC catalysts calculated by the DFT method. Most of the pores were observed in the range of 1.6–4.4 nm, and a small distribution was also observed at the pore size range above 4.4 nm, which confirmed predominantly mesopore and some micropore presence in the carbon. However, the textural pore structure of CL-derived NPC, Pd/NPC, Ni/NPC, and PdNi/NPC catalysts are reported in Table 3. The S_{BET} of studied catalysts (i.e., 2037.34 m^2g^{-1} for Pd/NPC, 2142.16 m^2g^{-1} for Ni/NPC, 2187.96 m^2g^{-1} for PdNi/NPC) were significantly higher than NPC (2002.12 m2g-1) since the metallic particles also have a porous structure, resulting in increasing the total specific surface area of the catalyst, as depicted in Table 3. This finding agrees with the total pore volume, which was increased from 1.573 cm3g-1 for the NPC support to 1.601–1.730 cm^3g^{-1} for NPC-supported metal catalysts. Moreover, the studied catalysts are mainly composed of the mesoporous structure. This result is assured by the total mesopore volume (Table 3). Also, the average pore diameter of catalysts ranged between 2.71 and 2.96 nm, which is in the range of mesoporous structure.

XRD patterns of CL-derived NPC, Pd/NPC, Ni/NPC, and PdNi/NPC catalysts are shown in Fig. 9. NPC showed broad peaks at 24° and 43.5° assigned to (002) and (100), corresponding to the planes of carbon materials (Kan et al., 2017) exhibited in nanoporous carbon support. These broad peaks clearly showed the amorphous carbon structure and disordered arrangement of the carbon rings. The exhibited peaks at 40, 46.5, and 68.5 were assigned to (111), (200), and (220) planes of the metallic form of Pd, whereas the Ni metal peaks exhibited at 44.8, 52.4 and 74.12 were assigned to (111), (200) and (220) planes. The

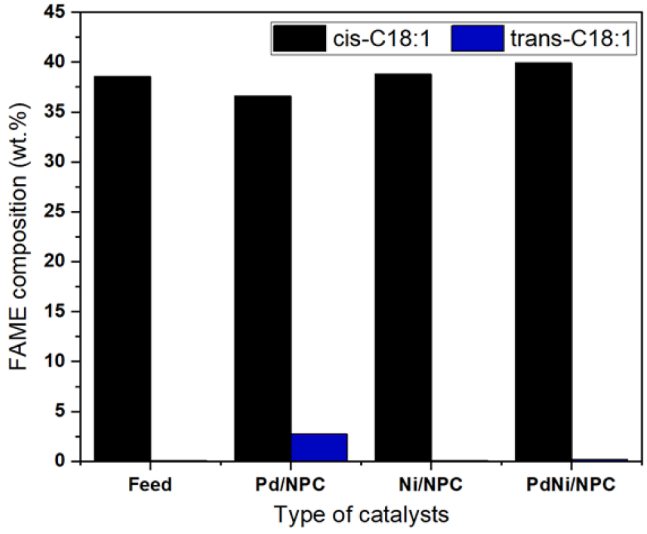

Fig. 11. Effect of catalyst type on cis/*trans*-isomer of C18:1 composition (reaction temperature = 100 °C, H_2 pressure = 4 bar and reaction time = 4 h).

diffraction peak of metallic exhibited in monometallic and bimetallic catalysts confirmed that the metal has been loaded on the surface of the NPC.

3.2. Partial hydrogenation of palm biodiesel feedstock (Palm BDF)

The conversion of C18:2 and biodiesel properties of palm BDF and palm H-FAMEs are shown in Table 4, while the detail of C18 composition is exhibited in Fig. 10. The conversion of C18:2 increased this way, PdNi/NPC > Pd/NPC > Ni/NPC catalysts, indicating that the bimetallic PdNi was slightly more active than monometallic Pd and Ni catalysts. Although the Ni catalyst showed less catalytic activity for the monometallic, it exhibited a high selectivity to the cis isomer of the C18:1 product compared with the Pd catalyst, as shown in Fig. 11. However, the Ni/NPC catalyst demonstrated high selectivity for the *cis*-C18:1 isomer. Furthermore, bimetallic PdNi/NPC catalysts outperformed monometallic catalysts due to their higher catalytic activity and increased *cis*-C18:1 composition due to the synergistic effect of active species. Interestingly, the highest activity and selectivity to *cis*-C18:1

Table 5
Current utilization of bimetallic in the biofuel production.

Metal catalyst	Support material	Reaction	Product	Ref
PdPt	MCM-41 mesoporous SiO_2	Partial hydrogenation	H-FAMEs (Soybean oil)	(Na Rungsi et al., 2021)
PdNi	Carbon from recycled polymer	Partial hydrogenation	H-FAMEs (Soybean oil)	(Fiore et al., 2022)
PdNi	Amined-Lapindo mud	Hydrotreatment	Liquid hydrocarbon	(Trisunaryanti et al., 2022)
CoMo	Bottom ash	Catalytic cracking	Liquid hydrocarbon	(Oktadina et al., 2023)
Ni, Pd, PdNi	NPC from biomass	Partial hydrogenation	H-FAMEs (Palm oil)	This study

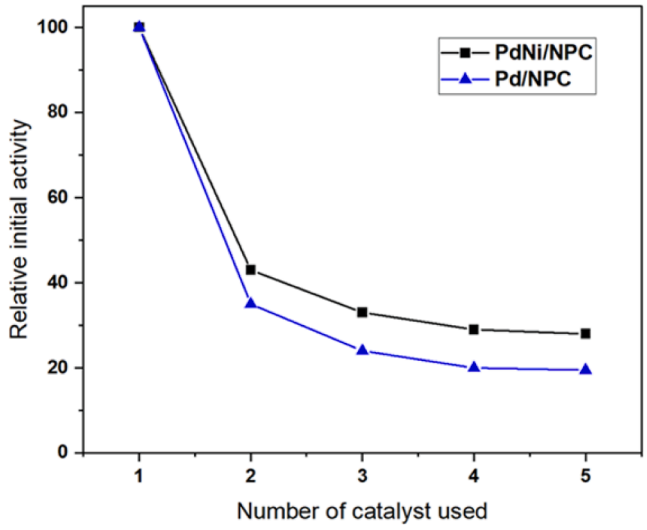

Fig. 12. Catalytic stability of Pd/NPC and PdNi/NPC catalyst (reaction temperature = 100 °C, H_2 pressure = 4 bar and reaction time = 4 h).

isomer were obtained over bimetallic PdNi catalyst, suggesting the synergistic effect between metallic Pd and Ni species (Chen et al., 2017; Gupta et al., 2020).

After partial hydrogenation of palm BDF, the oxidation stability of the H-FAME product using different catalysts was increased from 13.7 to 17.1 h for PdNi/NPC catalyst, 16.3 h for Pd/NPC catalyst and 14.1 h for Ni/NPC catalyst, in compliance with existing biodiesel standards including international standards EN14214 (>8h), ASTM D6751 (>3h) and Thai national standard (>10 h). Cloud points of all H-FAME products are in the range of 14–15 °C, which meets the Thai industrial recommendation (<16 °C) (Yusoff et al., 2021). However, the evaluation of supported bimetallic catalysts has been extensively studied for biofuel processing because of their exceptional catalytic reactivity. This finding is evident in the present trend of using bimetallic catalysts for biofuel synthesis, as shown in Table 5.

3.3. Catalyst deactivation and stability

Fig. 12 shows the deactivation study of Pd and Pd catalysts. The activity of Pd/NPC and PdNi/NPC catalysts decreased after the second use, and the activity decreased slowly afterward until it remained almost stable to the fifth run. It was shown that the PdNi/NPC catalyst exhibited higher catalytic activity compared with the Pd/NPC catalyst. To explain catalyst deactivation, the PdNi/NPC catalyst morphology after partial hydrogenation reaction at a reaction temperature of 100 °C and H_2 pressure of 4 bar was analyzed in Fig. 13. After partial hydrogenation, the SEM micrograph of the used catalyst exhibited no significant change in catalyst morphology compared to the fresh catalyst. BET surface area and metal dispersion of the PdNi/NPC catalyst before and after partial hydrogenation were further investigated and summarized in Table 6. The surface area of the fresh catalyst and used catalyst after the reaction at 100 °C for 4 bar exhibited S_{BET} at 2139 m^2g^{-1} and 2127 m^2g^{-1}, respectively. This result indicated that the textural property did not significantly change after the reaction. After partial hydrogenation, the dispersion of active metal species gradually decreased from 48.53 % to 23.94 % by approximately a 50 % drop in comparison with the fresh catalyst due to active metal covered by reactant and products during the reaction accompanied by an agglomeration of metal (Boldrini et al., 2015).

4. Conclusions

The cattail leaf-derived NPC was successfully synthesized via hydrothermal carbonization and KOH activation with very high porosity, mostly in mesopores, and a high S_{BET} of 2002.12 m^2g^{-1}. The NPC was used to support the development of monometallic Pd/NPC and Ni/NPC, as well as bimetallic PdNi/NPC catalysts for the partial hydrogenation reaction of palm biodiesel to H-FAME. The high porosity of NPC supported improved the dispersion of nanometal catalyst. The monometallic Pd/NPC catalyst exhibited significantly higher catalytic activity than the transition metal Ni/NPC catalyst. However, Ni/NPC catalyst showed favorable selectivity for the *cis*-C18:1 isomer. Besides bimetallic PdNi/NPC outperformed the monometallic catalysts due to the highest

Table 6
BET surface area and metal dispersion of fresh and 5th used PdNi/NPC catalysts.

Sample	S_{BET} (m^2g^{-1})	Metal dispersion (%)
Fresh catalyst	2139	48.53
5^{th}used catalyst	2127	23.94

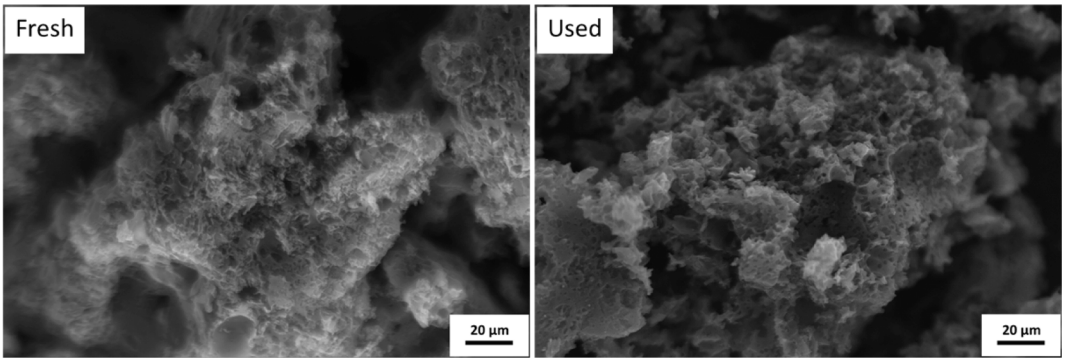

Fig. 13. Scanning electron microscope (SEM) micrographs of fresh and used PdNi/NPC catalysts at 500x magnification.

catalytic activity and the increasing composition of *cis*-C18:1 from the synergistic effect of active species. The presence of Ni in the bimetallic PdNi/NPC catalyst effectively reduced the deactivation of the catalyst. In addition, the oxidation stability of palm biodiesel feedstock increased from 13.69 to 17.12 h. The combination between noble and transition metal significantly exhibited a superior catalyst activity for the partial hydrogenation of biodiesel. Therefore, the upgrading of H-FAME through the partial hydrogenation of palm biodiesel is a beneficial for utilization of biofuel in a high blending ratio for diesel engine.

CRediT authorship contribution statement

Tripob Longprang: Conceptualization, Formal analysis, Investigation, Methodology, Writing – original draft. **Napat Kaewtrakulchai:** Conceptualization, Formal analysis, Investigation, Methodology, Writing – original draft. **Worapon Kiatkittipong:** Supervision, Writing – review & editing. **Atthapon Srifa:** Supervision, Writing – review & editing. **Nuwong Chollacoop:** Funding acquisition, Resources, Supervision. **Apiluck Eiad-Ua:** Resources, Supervision, Writing – review & editing. **Suttichai Assabumrungrat:** Funding acquisition, Supervision, Writing – review & editing.

Declaration of competing interest

The authors declare that they have no known competing financial interests or personal relationships that could have appeared to influence the work reported in this paper.

Acknowledgements

The authors would like to acknowledge the support from Thailand Graduate Institute of Science and Technology (TGIST) and the Research Chair Grant from National Science and Technology Development Agency (NSTDA), Material Analytical Instrument Service Unit (NMIS), College of Materials Innovation and Technology, King Mongkut's Institute of Technology Ladkrabang, Kasetsart Agricultural and Agro-Industrial Product Improvement Institute, Kasetsart University, and Patum Vegetable Oil Company Limited (PVO), Thailand, for providing biodiesel feedstock.

References

Abdalla, E.M., Hassan, S.S., Elganzory, H.H., Aly, S.A., Alshater, H., 2021. Molecular docking, DFT calculations, effect of high energetic ionizing radiation, and biological evaluation of some novel metal (II) heteroleptic complexes bearing the thiosemicarbazone ligand. Molecules 26 (19).

Adira Wan Khalit, W.N., Marliza, T.S., Asikin-Mijan, N., Gamal, M.S., Saiman, M.I., Ibrahim, M.L., Taufiq-Yap, Y.H., 2020. Development of bimetallic nickel-based catalysts supported on activated carbon for green fuel production. RSC Adv. 10 (61), 37218–37232.

Adu-Mensah, D., Mei, D., Zuo, L., Zhang, Q., Wang, J., 2019. A review on partial hydrogenation of biodiesel and its influence on fuel properties. Fuel 251, 660–668.

Ahmad, K., Nazir, M.A., Qureshi, A.K., Hussain, E., Najam, T., Javed, M.S., Shah, S.S.A., Tufail, M.K., Hussain, S., Khan, N.A., Shah, H.-U.-R., Ashfaq, M., 2020. Engineering of Zirconium based metal-organic frameworks (Zr-MOFs) as efficient adsorbents. Mater. Sci. Eng. B, 262.

Alshater, H., Al-Sulami, A.I., Aly, S.A., Abdalla, E.M., Sakr, M.A., Hassan, S.S., 2023. Antitumor and antibacterial activity of Ni(II), Cu(II), Ag(I), and Hg(II) complexes with ligand derived from thiosemicarbazones: Characterization and theoretical studies. Molecules 28 (6).

Aly, S.A., Elembaby, D., 2020. Synthesis, spectroscopic characterization and study the effect of gamma irradiation on VO2+, Mn2+, Zn2+, Ru3+, Pd2+, Ag+ and Hg2+ complexes and antibacterial activities. Arab. J. Chem. 13 (2), 4425–4447.

Aly, S.A., Fathalla, S.K., 2020. Preparation, characterization of some transition metal complexes of hydrazone derivatives and their antibacterial and antioxidant activities. Arab. J. Chem. 13 (2), 3735–3750.

Arana, J., Dona-Rodrıguez, J., Rendón, E.T., i Cabo, C.G., González-Dıaz, O., Herrera-Melián, J., Pérez-Peña, J., Colón, G., Navıo, J., 2003. TiO2 activation by using activated carbon as a support: Part II. Photoreactivity and FTIR study. Appl Catal B 44 (2), 153–160.

Boldrini, D.E., Tonetto, G.M., Damiani, D.E., 2015. Experimental study of the deactivation of Pd on anodized aluminum monoliths during the partial hydrogenation of vegetable oil. Chem. Eng. J. 270, 378–384.

Boreskov, G.K., 2003. Heterogeneous catalysis. Nova Publishers.

Chanpee, S., Kaewtrakulchai, N., Khemasiri, N., Eiad-Ua, A., Assawasaengrat, P., 2022. Nanoporous carbon from oil palm leaves via hydrothermal carbonization-combined KOH Activation for paraquat removal. Molecules 27 (16).

Chen, B., Li, F., Huang, Z., Yuan, G., 2017. Carbon-coated Cu-Co bimetallic nanoparticles as selective and recyclable catalysts for production of biofuel 2, 5-dimethylfuran. Appl Catal B 200, 192–199.

Dizbay-Onat, M., Vaidya, U.K., Lungu, C.T., 2017. Preparation of industrial sisal fiber waste derived activated carbon by chemical activation and effects of carbonization parameters on surface characteristics. Ind. Crop. Prod. 95, 583–590.

Douvartzides, S.L., Charisiou, N.D., Papageridis, K.N., Goula, M.A., 2019. Green diesel: Biomass feedstocks, production technologies, catalytic research. Fuel Properties and Performance in Compression Ignition Internal Combustion Engines Energies 12 (5).

Edvardsson, J., Rautanen, P., Littorin, A., Larsson, M., 2001. Deactivation and coke formation on palladium and platinum catalysts in vegetable oil hydrogenation. J. Am. Oil Chem. Soc. 78 (3), 319–327.

Eugenio Quaranta, A.D., Colucci, A., Cornacchia, D., 2022. Partial hydrogenation of FAMEs with high content of C18:2 dienes. Selective hydrogenation of tobacco seed oil-derived biodiesel. Fuel 326, 125030.

Fiore, A.M., Romanazzi, G., Leonelli, C., Mastrorilli, P., Dell'Anna, M.M., 2022. Partial hydrogenation of soybean and waste cooking oil biodiesel over recyclable-polymer-supported Pd and Ni nanoparticles. Catalysts 12 (5).

González-Castaño, M., le Saché, E., Berry, C., Pastor-Pérez, L., Arellano-García, H., Wang, Q., Reina, T., 2021. Nickel phosphide catalysts as efficient systems for CO2 upgrading via dry reforming of methane. Catalysts 11 (4).

Gupta, D., Kumar, R., Pant, K.K., 2020. Hydrotalcite supported bimetallic (Ni-Cu) catalyst: A smart choice for one-pot conversion of biomass-derived platform chemicals to hydrogenated biofuels. Fuel 277, 118111.

Hosny, S., Shehata, M.R., Aly, S.A., Alsehli, A.H., Salaheldeen, M., Abu-Dief, A.M., Abu-El-Wafa, S.M., 2024. Designing of novel nano-sized coordination compounds based on Spinacia oleracea extract: Synthesis, structural characterization, molecular docking, computational calculations, and biomedical applications. Inorg. Chem. Commun. 160.

Huang, X., Kudo, S., Ashik, U.P.M., Einaga, H., Hayashi, J.-I., 2020. Selective hydrodeoxygenation of γ-valerolactone over silica-supported Rh-based bimetallic catalysts. Energy Fuel 34 (6), 7190–7197.

Huang, D., Zhou, H., Lin, L., 2012. Biodiesel: an alternative to conventional fuel. Energy Procedia 16, 1874–1885.

Jadsadajerm, S., Wannapeera, J., Phopiyanukror, A., Worasuwannarak, N., 2024. Influence of oxygen concentration on torrefaction of Leucaena: gas formation rates and chemical properties analysis. Biomass Convers. Biorefin.

Jaruwat, D., Udomsap, P., Chollacoop, N., Fuji, M., Eiad-ua, A., 2018. Effects of hydrothermal temperature and time of hydrochar from Cattail leaves. In: *AIP Conference Proceedings*. AIP Publishing LLC, p. 020016.

Kaewtrakulchai, N., Kaewmeesri, R., Itthibenchapong, V., Eiad-Ua, A., Faungnawakij, K., 2020. Palm oil conversion to bio-jet and green diesel fuels over cobalt phosphide on porous carbons derived from palm male flowers. Catalysts 10 (6).

Kaewtrakulchai, N., Fuji, M., Eiad-Ua, A., 2022a. Catalytic deoxygenation of palm oil over metal phosphides supported on palm fiber waste derived activated biochar for producing green diesel fuel. RSC Adv 12 (40), 26051–26069.

Kaewtrakulchai, N., Smuthkochorn, A., Manatura, K., Panomsuwan, G., Fuji, M., Eiad-Ua, A., 2022b. Porous biochar supported transition metal phosphide catalysts for hydrocracking of palm oil to bio-jet fuel. Materials (basel) 15 (19).

Kaewtrakulchai, N., Chanpee, S., Manatura, K., Eiad-Ua, A., 2023. Upgrading of corn stalk residue and tannery waste into sustainable solid biofuel via conventional hydrothermal carbonization and co-hydrothermal carbonization. Journal of Sustainability Research 5 (3).

Kaewtrakulchai, N., Chanpee, S., Jadsadajerm, S., Wongrerkdee, S., Manatura, K., Eiad-Ua, A., 2024. Co-hydrothermal carbonization of polystyrene waste and maize stover combined with KOH activation to develop nanoporous carbon as catalyst support for catalytic hydrotreating of palm oil. Carbon Resources Conversion 7 (4).

Kan, Y., Yue, Q., Li, D., Wu, Y., Gao, B., 2017. Preparation and characterization of activated carbons from waste tea by H3PO4 activation in different atmospheres for oxytetracycline removal. J. Taiwan Inst. Chem. Eng. 71, 494–500.

Knothe, G., 2010. Biodiesel and renewable diesel: a comparison. Prog. Energy Combust. Sci. 36 (3), 364–373.

Lee, A.F., Wilson, K., 2015. Recent developments in heterogeneous catalysis for the sustainable production of biodiesel. Catal. Today 242, 3–18.

Li, S., Han, K., Li, J., Li, M., Lu, C., 2017. Preparation and characterization of super activated carbon produced from gulfweed by KOH activation. Microporous Mesoporous Mater. 243, 291–300.

Manić, N.G., Janković, B.Ž., Stojiljković, D.D., Jovanović, V.V., Radojević, M.B., 2019. TGA-DSC-MS analysis of pyrolysis process of various agricultural residues. Therm. Sci. 23 (Suppl. 5), 1457–1472.

Manoj, B., Kunjomana, A., 2012. Study of stacking structure of amorphous carbon by X-ray diffraction technique. Int. J. Electrochem. Sci 7 (4), 3127–3134.

Murugesan, A., Umarani, C., Subramanian, R., Nedunchezhian, N., 2009. Bio-diesel as an alternative fuel for diesel engines—a review. Renew. Sustain. Energy Rev. 13 (3), 653–662.

Na Rungsi, A., Truong, T.H., Thunyaratchatanon, C., Luengnaruemitchai, A., Chollacoop, N., Chen, S.-Y., Mochizuki, T., Takagi, H., Yoshimura, Y., 2021. Tuning the porosity of sulfur-resistant Pd-Pt/MCM-41 bimetallic catalysts for partial hydrogenation of soybean oil-derived biodiesel. Fuel 298.

Nabi, M.N., Akhter, M.S., Shahadat, M.M.Z., 2006. Improvement of engine emissions with conventional diesel fuel and diesel–biodiesel blends. Bioresour. Technol. 97 (3), 372–378.

Naderi, M. 2015. Surface Area: Brunauer–Emmett–Teller (BET). in: *Progress in filtration and separation*, Elsevier, pp. 585-608.
Naseem, K., Ahmad, K., Anwar, A., Farooqi, Z.H., Najeeb, J., Iftikhar, M.A., Hassan, W., Batool, A.U., Haider, S., Akhtar, M.S., 2023. Raphanus caudatus biomass powder as potential adsorbent for the removal of crystal violet and Rhodamine B dye from wastewater. Z. Phys. Chem. 237 (11), 1863–1883.
Nelson, W.L., 2018. Petroleum refinery engineering. McGraw-Hill.
Numwong, N., Luengnaruemitchai, A., Chollacoop, N., Yoshimura, Y., 2013. Effect of metal type on partial hydrogenation of rapeseed oil-derived FAME. J. Am. Oil Chem. Soc. 90 (9), 1431–1438.
Panomsuwan, G., Hussakan, C., Kaewtrakulchai, N., Techapiesancharoenkij, R., Serizawa, A., Ishizaki, T., Eiad-Ua, A., 2022. Nitrogen-doped carbon derived from horse manure biomass as a catalyst for the oxygen reduction reaction. RSC Adv 12 (27), 17481–17489.
Piccolo, L., Kibis, L., 2015. The partial hydrogenation of butadiene over Al13Fe4: A surface-science study of reaction and deactivation mechanisms. J. Catal. 332, 112–118.
Puna, J., Gomes, J., Correia, M.J.N., Dias, A.S., Bordado, J., 2010. Advances on the development of novel heterogeneous catalysts for transesterification of triglycerides in biodiesel. Fuel 89 (11), 3602–3606.
Putri Afifa Nur Oktadina, A.S., Yerizam, Muhammad, Medi, Ali, 2023. Journal of mechanical, civil and industrial engineering. Journal of Mechanical, Civil and Industrial, Engineering 37–42.
Quaranta, E., Cornacchia, D., 2020. Partial hydrogenation of a C18: 3-rich FAME mixture over Pd/C. Renew. Energy.
Roy, P., Jahromi, H., Adhikari, S., Zou Finfrock, Y., Rahman, T., Ahmadi, Z., Mahjouri-Samani, M., Feyzbar-Khalkhali-Nejad, F., Oh, T.-S., 2022. Performance of biochar assisted catalysts during hydroprocessing of non-edible vegetable oil: Effect of transition metal source on catalytic activity. Energ. Conver. Manage. 252.
Satterfield, C.N. 1991. Heterogeneous catalysis in industrial practice.
Shin, S., Jang, J., Yoon, S.-H., Mochida, I., 1997. A study on the effect of heat treatment on functional groups of pitch based activated carbon fiber using FTIR. Carbon 35 (12), 1739–1743.
Siddiqui, M.T.H., Baloch, H.A., Nizamuddin, S., Mubarak, N.M., Hossain, N., Zavabeti, A., Mazari, S.A., Griffin, G.J., Srinivasan, M., 2021. Synthesis and optimization of chitosan supported magnetic carbon bio-nanocomposites and bio-oil production by solvothermal carbonization co-precipitation for advanced energy applications. Renew. Energy 178, 587–599.
Sinfelt, J.H., 1985. Bimetallic catalysts. Sci. Am. 253 (3), 90–101.
Stathis, P., Stavroulaki, D., Kaika, N., Krommyda, K., Papadogianakis, G., 2017. Low trans-isomers formation in the aqueous-phase Pt/TPPTS-catalyzed partial hydrogenation of methyl esters of linseed oil. Appl Catal B 209, 579–590.
Studentschnig, A.F.H., Schober, S., Mittelbach, M., 2015. Partial hydrogenation of fish oil methyl esters for the production of biofuels. Energy Fuel 29 (6), 3776–3779.
Tang, S., Zhang, Z., Xiang, J., Yang, X., Shen, X., Song, F., 2022. Recent advances in transition metal nitrides for hydrogen electrocatalysis in alkaline media: From catalyst design to application. Front Chem 10, 1073175.
Thunyaratchatanon, C., Luengnaruemitchai, A., Jitjamnong, J., Chollacoop, N., Chen, S.-Y., Yoshimura, Y., 2018. Influence of alkaline and alkaline earth metal promoters on the catalytic performance of Pd–M/SiO2 (M= Na, Ca, or Ba) catalysts in the partial hydrogenation of soybean oil-derived biodiesel for oxidative stability improvement. Energy Fuel 32 (9), 9744–9755.
Toshima, N., Yonezawa, T., 1998. Bimetallic nanoparticles—novel materials for chemical and physical applications. New J. Chem. 22 (11), 1179–1201.
Tran, C.-C., Akmach, D., Kaliaguine, S., 2020. Hydrodeoxygenation of vegetable oils over biochar supported bimetallic carbides for producing renewable diesel under mild conditions. Green Chem. 22 (19), 6424–6436.
Trisunaryanti, W., Alethiana, A., Falah, I.I., Fatmawati, D.A., 2022. Effective production of biofuel from used cooking oil over Ni–Pd loaded on amine-functionalized Lapindo Mud catalyst. React. Kinet. Mech. Catal. 135 (2), 951–970.
Tseng, R.-L., Tseng, S.-K., Wu, F.-C., Hu, C.-C., Wang, C.-C., 2008. Effects of micropore development on the physicochemical properties of KOH-activated carbons. J. Chin. Inst. Chem. Eng, 39 (1), 37–47.
Turrio-Baldassarri, L., Battistelli, C.L., Conti, L., Crebelli, R., De Berardis, B., Iamiceli, A. L., Gambino, M., Iannaccone, S., 2004. Emission comparison of urban bus engine fueled with diesel oil and 'biodiesel'blend. Sci. Total Environ. 327 (1–3), 147–162.
Udomsap, P., Meesiri, S., Chollacoop, N., Eiad-Ua, A., 2021. Biomass nanoporous carbon-supported Pd catalysts for partial hydrogenation of biodiesel: Effects of surface chemistry on Pd particle size and catalytic performance. Nanomaterials 11 (6), 1431.
Vedaraman, N., Puhan, S., Nagarajan, G., Velappan, K., 2011. Preparation of palm oil biodiesel and effect of various additives on NOx emission reduction in B20: An experimental study. Int. J. Green Energy 8 (3), 383–397.
Vignesh, P., Pradeep Kumar, A.R., Ganesh, N.S., Jayaseelan, V., Sudhakar, K., 2021. Biodiesel and green diesel generation: an overview. Oil & Gas Science and Technology – Revue d'IFP Energies Nouvelles 76.
Wang, F., Xu, J., Jiang, J., Liu, P., Li, F., Ye, J., Zhou, M., 2018. Hydrotreatment of vegetable oil for green diesel over activated carbon supported molybdenum carbide catalyst. Fuel 216, 738–746.
Xiang, X., Liu, E., Li, L., Yang, Y., Shen, H., Huang, Z., Tian, Y., 2011. Activated carbon prepared from polyaniline base by K 2 CO 3 activation for application in supercapacitor electrodes. J. Solid State Electrochem. 15 (3), 579–585.
Yao, Z., Ma, X., Wu, Z., Yao, T., 2017. TGA–FTIR analysis of co-pyrolysis characteristics of hydrochar and paper sludge. J. Anal. Appl. Pyrol. 123, 40–48.
Yusoff, M.N.A.M., Zulkifli, N.W.M., Sukiman, N.L., Chyuan, O.H., Hassan, M.H., Hasnul, M.H., Zulkifli, M.S.A., Abbas, M.M., Zakaria, M.Z., 2021. Sustainability of palm biodiesel in transportation: a review on biofuel standard, policy and international collaboration between Malaysia and Colombia. Bioenergy Res. 14 (1), 43–60.
Zhu, Q.-L., Song, F.-Z., Wang, Q.-J., Tsumori, N., Himeda, Y., Autrey, T., Xu, Q., 2018. A solvent-switched in situ confinement approach for immobilizing highly-active ultrafine palladium nanoparticles: boosting catalytic hydrogen evolution. J. Mater. Chem. A 6 (14), 5544–5549.